

## DEEP IMAGING OF THE KUIPER BELT WITH THE KECK 10 METER TELESCOPE

JANE X. LUU<sup>1</sup>

Astronomy Department, Harvard University, 60 Garden Street, Cambridge, MA 02138

AND

DAVID C. JEWITT<sup>1</sup>

Institute for Astronomy, 2680 Woodlawn Drive, Honolulu, HI 96822

Received 1998 April 27; accepted 1998 May 19; published 1998 July 1

### ABSTRACT

We present a new, pencil-beam survey of the Kuiper Belt taken with the Keck 10 m telescope. The cumulative surface density of Kuiper Belt Objects measured to apparent red magnitude  $m_R = 26.1$  is  $31^{+12}_{-14} \text{ deg}^{-2}$ , while to  $m_R = 26.6$  it is  $40 \pm 33 \text{ deg}^{-2}$ . These numbers are compatible with an extrapolation of the luminosity function deduced earlier from measurements in the  $20 \leq m_R \leq 25$  range, and they confirm a Kuiper Belt differential size distribution index  $q \sim 4$ .

*Subject headings:* comets: general — solar system: formation

### 1. INTRODUCTION

The solar system beyond Neptune contains a rich assortment of planetary bodies collectively known as Kuiper Belt Objects (KBOs). Recent ground-based measurements have revealed more than 60 KBOs (as of 1998 April), with diameters ranging from the limits of detection near 100 km up to 800 km (Jewitt & Luu 1993, 1995, hereafter JL95; Irwin, Tremaine, & Zytzkow 1995; Williams et al. 1995; Jewitt, Luu, & Chen 1996, hereafter JLC96; Gladman & Kavelaars 1997; Luu et al. 1997; Jewitt, Luu, & Trujillo 1998, hereafter JLT98). The cumulative luminosity function (CLF) of the Kuiper Belt is one of the most important measurable quantities because, in magnitude-limited surveys, it reflects both the size distribution and the radial distance distribution of the KBOs. Through models, the CLF may be used to constrain the size and distance distributions. The size distribution is important because it may tell us about the conditions in which the KBOs grew (Stern & Colwell 1997; Kenyon & Luu 1998) as well as about subsequent collisional modification (Farinella & Davis 1996). The distance distribution carries additional information about accretion and about the dynamical evolution of the Kuiper Belt in the 4.6 Gyr since formation (see, e.g., Holman & Wisdom 1993; Duncan, Levison, & Budd 1995; Malhotra 1996). The CLF is well determined in the magnitude range  $20 \leq m_R \leq 25$  (JLT98) and is described by

$$\log [\Sigma(m_R)] = \alpha(m_R - m_0), \quad (1)$$

where  $\alpha = 0.58 \pm 0.05$  and  $m_0 = 23.27 \pm 0.11$  (JLT98). KBOs brighter than  $m_R = 20$  are relatively rare and await detection by wide-field surveys that are currently underway. Objects fainter than  $m_R = 25$  are potentially very numerous but have not yet been the subject of a concerted ground-based observational effort (a reported measurement of these objects with the *Hubble Space Telescope* is discussed later). In this Letter, we present new measurements of the surface density of KBOs fainter than  $m_R = 25$ .

### 2. OBSERVATIONS

Observations were taken at the Keck 10 m telescope on a range of dates from 1994 to 1996 (see Table 1) using the LRIS charge-coupled device (CCD) camera (Oke et al. 1995). We used LRIS in imaging mode with an  $R$  filter and a standard integration time per image of 900 s. In 900 s, an object moving at  $3'' \text{ hr}^{-1}$  will trail by  $0''.75$ , producing a trailing loss of  $\sim 0.2$  mag in seeing of  $0''.75$  full width at half-maximum (FWHM) (see, e.g., Tancredi & Lindgren 1994). The LRIS image scale is  $0''.215 \text{ pixel}^{-1}$ . We used the central  $1600 \times 2040$  pixels ( $41.9 \text{ arcmin}^2$ ) of the field of view to avoid partially vignetted regions near the edge. The seeing was carefully monitored during the integrations, and the alignment of the primary mirror segments was periodically adjusted using the IMALIGN algorithm. Photometric calibration of the data was obtained through observations of faint standards (Landolt 1992).

Two separate strategies were used to secure the data. For the “medium-deep” survey, we used the usual technique of imaging each field 3 times in order to detect KBOs by virtue of their motion relative to the fixed stars. In total, we observed 24 medium-deep fields ( $1007.0 \text{ arcmin}^2$ ) in average seeing that varied from  $0''.75$  to  $0''.93$  FWHM.

For the “ultra-deep” survey, we recorded a continuous series of images of a single field throughout each night. The images were dithered so as to eliminate possible problems caused by defective pixels (thus reducing the effective area further). Images from the series were then combined to make three ultra-deep images per field, each having effective integration time  $\sim 4500$  s, which were then searched for KBOs. The image combinations were made assuming a grid of KBO rates in the range  $1''.5\text{--}3''.3 \text{ hr}^{-1}$  west,  $0''.7\text{--}1''.3 \text{ hr}^{-1}$  north, with grid spacings of  $0''.3 \text{ hr}^{-1}$ . These rates were chosen to encompass the 37–80 AU distance range where we expect to find objects. The  $0''.3 \text{ hr}^{-1}$  grid spacing was selected empirically so that we would not miss any KBO in the 37–80 AU heliocentric range. From experiments with both real and artificial KBOs, we found that we could tolerate a rate error of  $0''.3 \text{ hr}^{-1}$  without loss of sensitivity. In total, we observed three ultra-deep fields (combined area  $101.2 \text{ arcmin}^2$ ), with average seeing each night near  $0''.75$  FWHM.

Photometry was performed using a circular aperture 10 pixels ( $2''.1$ ) in diameter, with sky subtraction from a contiguous annulus of 30 pixels ( $6''.5$ ) outer diameter. Experiments with

<sup>1</sup> Visiting Astronomer, W. M. Keck Observatory, jointly operated by California Institute of Technology and the University of California.

TABLE 1  
JOURNAL OF OBSERVATIONS

UT Date <sup>a</sup>	FWHM <sup>b</sup> (pixel)	N <sup>c</sup>	$m_R(50)^d$ (mag)	Total Area <sup>e</sup> (arcmin <sup>2</sup> )	Object <sup>f</sup>
1994 Sep 05 .....	0.75 ± 0.02	1 × 15	26.6	33.1	
1995 Mar 23 .....	0.80 ± 0.01	1 × 19	26.6	31.5	K-UD
1995 Mar 24 .....	0.75 ± 0.02	1 × 17	26.6	36.6	
1995 Nov 18 .....	0.93 ± 0.06	3 × 3	26.0	125.9	1995 WY2, K3
1995 Nov 19 .....	0.85 ± 0.05	4 × 3	26.1	167.8	
1996 Apr 20 .....	0.91 ± 0.03	3 × 3	26.0	125.9	
1996 Apr 21 .....	0.77 ± 0.03	8 × 3	26.2	335.7	K13, K15, K16
1996 Sep 12 .....	0.78 ± 0.03	2 × 3	26.2	83.9	
1996 Sep 13 .....	0.75 ± 0.02	4 × 3	26.2	167.8	

<sup>a</sup> UT date of the observations.

<sup>b</sup> Nightly mean and standard deviation on the mean of the seeing.

<sup>c</sup> Number of fields times number of integrations per field. For the ultra-deep survey, images with the worst seeing in each set were rejected, leaving 15 images per set.

<sup>d</sup> Limiting red magnitude, at which the detection efficiency falls to 50% of the peak value, as determined from simulations. All values are ±0.1 mag.

<sup>e</sup> Total nightly sky area surveyed.

<sup>f</sup> Objects discovered.

other aperture sizes showed photometric stability at the 0.1–0.3 mag level in the 26th mag range.

The limiting magnitudes of the survey observations were measured by searching for synthetic images of KBOs added randomly to the data. The synthetic KBOs all had Moffat profiles with  $\beta = 2.5$  (Moffat 1969) and were artificially trailed to simulate movement of the real KBOs during the 900 s integrations. We checked that the synthetic KBOs had shapes like those of real KBOs and that they were correctly photometrically scaled to the data. We generated KBOs of apparent magnitudes 25.3–27, with ~5 KBOs per 0.1 magnitude bin. The synthetic KBOs were “discovered” and measured using exactly the same procedures employed on real KBOs. From simulations with different values of the seeing,  $\theta$  (arcsec), we found that a probability of detection equal to 50% of the maximum was reached at red magnitude  $m_R(50) = (25.9 \pm 0.1) - 2.5 \log(\theta)$ . Thus, our best and worst medium-deep images have  $m_R(50) = 26.2 \pm 0.1$  (for  $\theta = 0''.75$ ) and  $26.0 \pm 0.1$  ( $\theta = 0''.93$ ), respectively. These are compatible with independent determinations of  $m_R(50)$  using LRIS data by Smail et al. (1995), when correctly scaled for differences in seeing, integration time, and trailing loss. Simulations of the medium-deep data gave  $m_R(50) = 26.1 \pm 0.1$ , and for the ultra-deep data  $m_R(50) = 26.6 \pm 0.1$  (Table 1).

### 3. DISCUSSION

We found six new KBOs in the combined Keck data; examples are shown in Figure 1. The properties of the new KBOs are listed in Table 2 (see Fig. 1). Except for 1995 WY2, each KBO was observed only on the night of discovery. For this reason, in principle, there is a small chance that the newly detected KBOs might be near-Earth asteroids, whose intrinsic motions coincidentally mimic the slow, retrograde movement expected of a KBO. With observations from only a short time-base on a single night, we are unable to eliminate this possibility from the absence of diurnal parallax in the normal way (JL95). However, in our other surveys we have not found such accidental slow movers, and it is highly unlikely that such objects might be found in the Keck data. We proceed on the assumption that the slow apparent motions are indicative of large geocentric distance.

Single-night observations of the newly detected KBOs provide only minimal constraints on their orbits. Experience with other single-night KBOs suggests that we can trust the distances

to the KBOs more than we can trust the other orbital parameters. The distances (Table 2) fall within the distance range defined by previously known KBOs. We compute diameters of KBOs under the assumption of uniform red geometric albedo,  $p_R = 0.04$  (see JLT98 for a discussion of this assumption). Limiting magnitude  $m_R = 26.1$  corresponds to an object diameter  $D_{0.04} \sim 80$  km at  $R = 50$  AU. Therefore, all KBOs in the line of sight with  $D_{0.04} \geq 80$  km and  $R \leq 50$  AU fall within the sensitivity limits of the Keck data. From  $\Sigma(m_R = 26.1) = 31 \text{ deg}^{-2}$  (Fig. 2) and a nominal ecliptic projected area  $A \sim 10^4 \text{ deg}^{-2}$  we find  $N = \Sigma A \sim 3.1 \times 10^5$  KBOs with  $D_{0.04} \geq 80$  km and  $R \leq 50$  AU. Scaled to  $D_{0.04} = 100$  km using a  $q = 4$  differential size distribution, we find  $N \sim 1.6 \times 10^5$ . This compares favorably with  $N \sim 7 \times 10^4$  based on earlier data (JLC98), which is good to no better than a factor of ~2 owing to, e.g., the poorly constrained inclination distribution. The consistent population estimates suggest that the large end of the KBO size distribution is well established. The mass of a  $q = 4$  distribution in which there are  $N$  objects larger than  $D_{\min}$  is

$$M = \frac{\pi \rho N D_{\min}^3}{2} \left( \frac{0.04}{p_R} \right)^{3/2} \ln \left( \frac{D_{\max}}{D_{\min}} \right), \quad (2)$$

where  $\rho$  is the bulk density and the size distribution extends to  $D_{\max}$ . We take  $p_R = 0.04$ ,  $D_{\min} = 100$  km,  $N = 1.6 \times 10^5$ ,  $\rho = 1000 \text{ kg m}^{-3}$ , and maximum object size equal to Pluto ( $D_{\max} = 2300$  km) to find  $M = 0.8 \times 10^{24} \text{ kg}$  (~0.1  $M_{\oplus}$ , where  $1 M_{\oplus} = 6 \times 10^{24} \text{ kg}$  is one Earth mass). Systematic uncertainties in the mass estimate arise from the density (factor of 2) and are dominated by the albedo term (factor of 10?). A safe conclusion would be that the mass of the observable objects in the Kuiper Belt is of order a few tenths of  $M_{\oplus}$ . The mass in smaller objects is observationally unconstrained. If the  $q = 4$  size distribution extends to 1 km, the total mass may be higher by a factor ~2 but still would be consistent with dynamical constraints, which limit the mass to be less than 1  $M_{\oplus}$  (Hamid, Marsden, & Whipple 1968).

The new cumulative surface densities are plotted in Figure 2. Also shown in Figure 2 is the fit to the CLF determined from observations in the range  $20 \leq m_R \leq 26.6$ , including the new Keck measurements (eq. [1]). Refitting the CLF yields the new parameters  $\alpha = 0.54 \pm 0.04$  and  $m_0 = 23.20 \pm 0.10$ . Observers using the *Hubble Space Telescope* (HST) (Cochran et

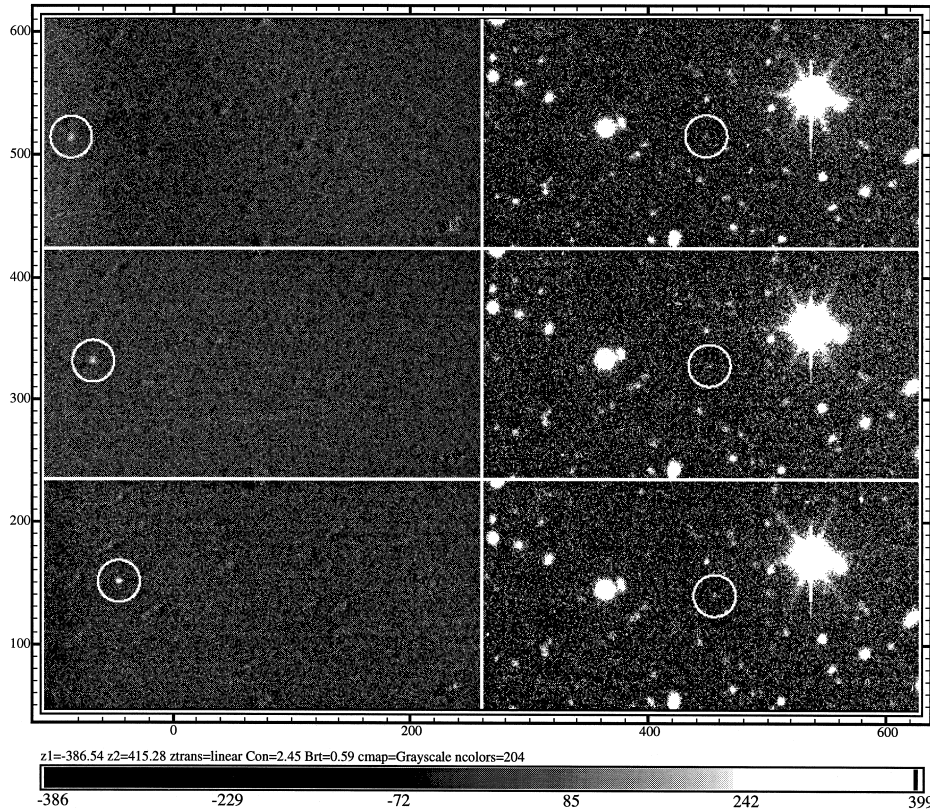


FIG. 1.—Images of two KBOs detected in this survey. The three left panels show the KBO K-UD ( $m_R \sim 25.0$ ) detected in the ultra-deep survey, while the three right panels show the KBO K15 ( $m_R \sim 25.7$ ) detected in the medium-deep survey. The panels are  $86'' \times 43''$ , with north to the top and east to the left. The white circle has projected diameter  $3.9''$ .

al. 1995) reported a high density of KBOs near the noise limit of the data at  $m_V \sim 28.6$  (corresponding to  $m_R \sim 28.1$  with  $V - R \approx 0.5$ ). This measurement has been criticized by Brown, Kulkarni, & Liggett (1997) on statistical grounds but was recently further defended by Cochran et al. (1998). The Cochran et al. (1995) datum lies above the extrapolated CLF by a factor of  $\sim 30$  (Fig. 2). There are at least three possible explanations for this discrepancy:

1. The fitted CLF may be in error. This seems unlikely, because the CLF has been determined from ground-based observations taken with different detectors, telescopes, and limiting magnitudes, with no evidence for significant discrepancies between independent measurements. In particular, a smooth fit from  $m_R = 24$  to  $m_R = 28.1$  would only be possible if the Keck data underestimated the number of KBOs by factors of  $\sim 11$  ( $m_R = 26.1$ ) and  $\sim 23$  ( $m_R = 26.6$ ), which seems unlikely.
2. The CLF may steepen between the Keck ( $m_R = 26.1$ , 26.6) and *HST* ( $m_R = 28.1$ ) limiting magnitudes. An increase in surface density by a factor of  $\sim 30$  relative to the fitted CLF (in the magnitude range 26.6 to 28.1) would be required to fit the *HST* determination.
3. The Cochran et al. datum may be in error, as suggested by Brown, Kulkarni, & Liggett (1997).

#### 4. SUMMARY

1. The cumulative surface densities of Kuiper Belt objects brighter than apparent red magnitude  $m_R = 26.1$  are  $31_{-14}^{+12} \text{ deg}^{-2}$  and  $40 \pm 33 \text{ deg}^{-2}$  at  $m_R = 26.6$ .
2. The cumulative luminosity function in the magnitude range  $20 \leq m_R \leq 26.6$  is well-fitted by equation (1) with  $\alpha =$

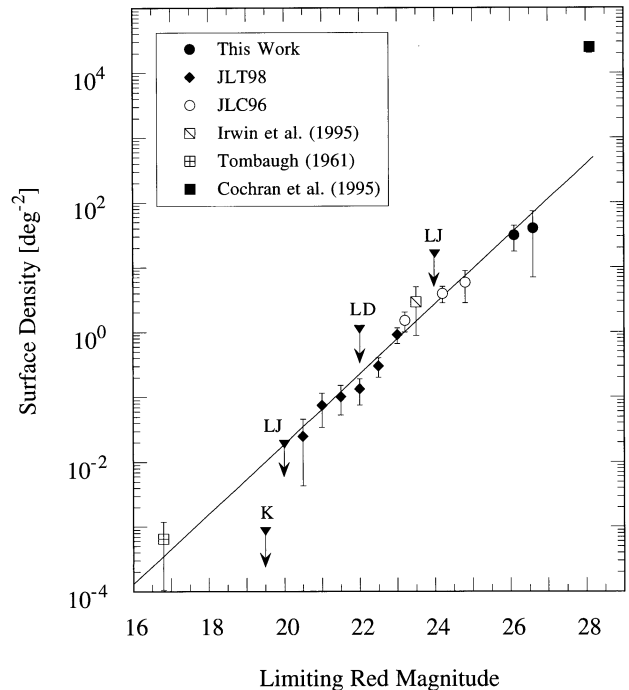


FIG. 2.—The plotted line is the fitted CLF, which includes the present Keck data and the Tombaugh (1961) data point, but not the upper limits (*inverted triangles*) or the Cochran et al. (1995) point.

TABLE 2  
PARAMETERS OF DISCOVERED KUIPER BELT OBJECTS

Name <sup>a</sup>	UT Date <sup>b</sup>	$d\alpha/dt^c$ (arcsec hr <sup>-1</sup> )	$d\delta/dt^d$ (arcsec hr <sup>-1</sup> )	$R^e$ (AU)	$D^f$ (AU)	$m_R^g$ (mag)	$m_R(1, 1, 0)^h$ (mag)	$D_{0.04}^i$ (km)
1995 WY2 .....	1995 Nov 18	2.9	0.2	47.76	46.85	23.8	7.0	206
K3 .....	1995 Nov 18	3.0	2.8	31	...	26.7	11.9	23
K13 .....	1996 Apr 21	1.2	2.4	48	...	26.4	9.6	63
K15 .....	1996 Apr 21	2.8	1.1	43	...	25.7	9.4	69
K16 .....	1996 Apr 21	3.1	0.6	40	...	25.9	9.9	55
KUD .....	1995 Mar 23	3.0	2.8	42	...	25.0	8.8	90

<sup>a</sup> Object name.

<sup>b</sup> UT date of the observation.

<sup>c</sup> R.A. rate. Estimated uncertainties caused by centroiding are  $\pm 0''.6$  hr<sup>-1</sup> ( $1\sigma$ ).

<sup>d</sup> Decl. rate. Estimated uncertainties caused by centroiding are  $\pm 0''.6$  hr<sup>-1</sup> ( $1\sigma$ ).

<sup>e</sup> Heliocentric distance at discovery.

<sup>f</sup> Geocentric distance at discovery.

<sup>g</sup> Apparent red magnitude. Photometric uncertainties range from  $\pm 0.1$  mag for the brightest objects, to  $\pm 0.3$  mag for the faintest.

<sup>h</sup> Red magnitude reduced to  $R = D = 1$  AU,  $\alpha = 0$ .

<sup>i</sup> Diameter computed assuming red geometric albedo = 0.04, phase angle = 0 deg, and  $D = R - 1$ , for all objects except of 1995 WY2.

$0.54 \pm 0.04$  and  $m_0 = 23.20 \pm 0.10$ . The mass of KBOs with diameters  $D_{0.04} \geq 100$  km and heliocentric distances  $R \leq 50$  AU is of order  $0.1 M_{\oplus}$ .

3. The surface density of Kuiper Belt objects at  $m_R = 28.1$  (Cochran et al. 1995) is a factor of  $\sim 30$  higher than the extrapolated cumulative luminosity function from ground-based data. Either the luminosity function is very much steeper

in the  $26.6 \leq m_R \leq 28.1$  magnitude interval or the *HST* datum is in error.

We thank Tom Bida for help with LRIS, Theresa Chelminiak for operating the Keck, and NASA for financial support of this work. We also thank Jan Kleyna for helpful discussions.

#### REFERENCES

- Brown, M. E., Kulkarni, S. R., & Liggett, T. J. 1997, *ApJ*, 490, L119  
 Cochran, A., Levison, H., Stern, S., & Duncan, M. 1995, *ApJ*, 455, 342  
 Cochran, A. L., Levison, H. F., Tamblin, P., Stern, S. A., & Duncan, M. J. 1998, *ApJL*, in press  
 Duncan, M., Levison, H. F., & Budd, S. M. 1995, *AJ*, 110, 3073  
 Farinella, P., & Davis, D. 1996, *Science*, 273, 938  
 Gladman, B., & Kavelaars, J. 1997, *A&A*, 317, 35  
 Hamid, S. E., Marsden, B., & Whipple, F. 1968, *AJ*, 73, 727  
 Holman, M., & Wisdom, J. 1993, *AJ*, 105, 1987  
 Irwin, M., Tremaine, S., & Zytlow, A. N. 1995, *AJ*, 110, 3082  
 Jewitt, D. C., & Luu, J. X. 1993, *Nature* 362, 730  
 ———. 1995, *AJ*, 109, 1867  
 Jewitt, D. C., Luu, J. X., & Chen, J. 1996, *AJ*, 112, 1225 (JLC96)  
 Jewitt, D. C., Luu, J. X., & Trujillo, C. 1998, *AJ*, 115, 2125 (JLT98)  
 Kenyon, S., & Luu, J. 1998, *AJ*, 115, 2136  
 Landolt, A. 1992, *AJ*, 104, 340  
 Luu, J. X., Marsden, B., Jewitt, D., Trujillo, C., Hergenrother, C., Chen, J., & Offutt, W. 1997, *Nature*, 387, 573  
 Malhotra, R. 1996, *AJ*, 111, 504  
 Moffat, A. F. J. 1969, *A&A*, 3, 455  
 Oke, J., et al. 1995, *PASP*, 107, 375  
 Smail, I., Hogg, D. W., Yan, L., & Cohen, J. 1995, *ApJ*, 449, L105  
 Stern, S. A., & Colwell, J. E. 1997, *AJ*, 114, 841  
 Tancredi, G., & Lindgren, M. 1994, *Icarus*, 107, 311  
 Tombaugh, C. W. 1961, in *Planets and Satellites*, ed. G. P. Kuiper & B. M. Middlehurst (Chicago: Univ. Chicago Press), 12  
 Williams, I. P., O'Ceallaigh, D. P., Fitzsimmons, A., & Marsden, B. G. 1995, *Icarus*, 116, 180